Lognormal mass distributions of nanodiamonds from proportionate vapor growth

Jochen Maul,[1,*] Edit Marosits,[2] Christa Sudek,[2] Thomas Berg,[1] and Ulrich Ott[2]

[1]*Institut für Physik, Staudingerweg 7, D-55129 Mainz, Germany*
[2]*Max Planck-Institut für Chemie, Becherweg 27, D-55128 Mainz, Germany*

For the investigation of the statistical growth behavior of diamond nanoparticles in vapor phase, a direct mass distribution determination was performed using laser ablation/ionization mass spectrometry. Different types of samples were investigated: cosmic diamonds of presolar origin found in meteorites, and larger synthetic diamonds obtained from vapor detonation processes. All samples exhibit lognormal mass distributions which are indicative for size-dependant (i.e., proportionate) molecular growth similar to chemical vapor depositionlike processes. The distribution parameters are extracted and discussed against the background of the statistical theory.

PACS number(s): 82.60.Qr, 82.20.−w, 05.70.−a

I. INTRODUCTION

The size distribution of small particles is an essential property of heterogeneously evolving systems. It comprises important information about both the prevailing thermodynamic conditions and the chemical environment, and hence provides basic insight into possible modes of particle formation. For natural growth processes which are unilaterally limited, e.g., due to vanishing particle radius, the size distribution is often found to be lognormal,[1] particularly when the accumulation behavior shows some proportionate effect.[2] Such processes appear in various fields, such as environmental sciences,[3] aerosol research,[4] biology,[5] or medical sciences.[6]

In this paper we demonstrate and discuss lognormal growth behavior on the basis of nanometer scale diamonds condensed from the vapor phase. Their mass distributions were recorded using laser ablation/ionization mass spectrometry. Different nanodiamond samples were analyzed originating from vapor phase reactions in different carbon-rich environments: cosmic diamonds most probably condensed in supernova ejecta (e.g., in Refs. 7 and 8), and synthetic ultradisperse diamonds (UDD) for comparison which were produced during detonation processes in vapor phase.[9]

Interstellar diamonds were predicted to exist in 1969 (Ref. 10) and were discovered in meteorites in 1987 (Ref. 7). They are two to three orders of magnitude smaller than other interstellar grains, found in meteorites such as silicon carbide and graphite (e.g., in Ref. 11), and represent the most abundant presolar fraction in primitive meteorites (e.g., in Ref. 8). Their presolar origin is indicated by the presence of noble gases with strongly anomalous isotopic compositions within them.[8,11]

Several mechanisms of formation were previously proposed for these diamonds: low-pressure condensation in expanding ejecta from supernovae,[7,12] high-pressure shock metamorphism of graphite[13] and irradiation of carbonaceous grains by either ultraviolet radiation or energetic particles.[14,15] Among them, condensation from the vapor phase, as it is characteristic for chemical vapor deposition (CVD) processes, turned out to be most likely. Indications were given both from their specific crystalline structure[16] and from

the fact that they are lognormally distributed in size[16,17] which points to CVD-like vapor absorption processes (e.g., in Refs. 1 and 18).

In previous works size distributions generally were obtained from the evaluation of transmission electron microscopic (TEM) images where single nanodiamonds were identified on the substrate for size estimation and for subsequent size statistics.[16,17] In this article we introduce a direct and model-independent mass distribution measurement by using laser ablation/ionization time-of-flight (TOF) mass spectrometry and apply it to both cosmic and synthetic nanodiamond samples (see, Fig. 1). Both types of diamonds show the same distribution behavior on a different mass scale, suggesting that both originate from similar physical formation processes. Application of a similar method, MALDI-TOF (i.e., matrix assisted laser desorption/ionization, where a "matrix" is added to the sample to enhance desorption/ionization), has been reported in an abstract by Lyon *et al.*[19,29] Our work differs from theirs in three ways: (a) in performing matrix-free ablation in order to avoid possible artifacts from chemical admixtures; (b) we investigated both cosmic and, for comparison, synthetic nanodiamonds, and (c) we also discuss physical implications with respect to the underlying statistical theory, pointing out possibilities of information extraction from such mass distribution measurements.

II. LOGNORMAL SIZE DISTRIBUTION

The statistical theory of the *logarithmo-normal* or simply *lognormal* size distribution was originally set down by McAlister in 1879.[20] Since then, theoretical understanding and wide applications have greatly increased, although it was believed for a long time that it is of less fundamental importance compared to the earlier formulated normal and binomial "sister distributions."

The lognormal distribution arises from a theory of elementary errors combined with a multiplicative process, just as the underlying change of growth is multiplicative rather than additive. In contrast to a constant (size-independent) growth process, where the particle radius r_j increases to the following time, resp. process step $j+1$ by a constant value,[2,21]
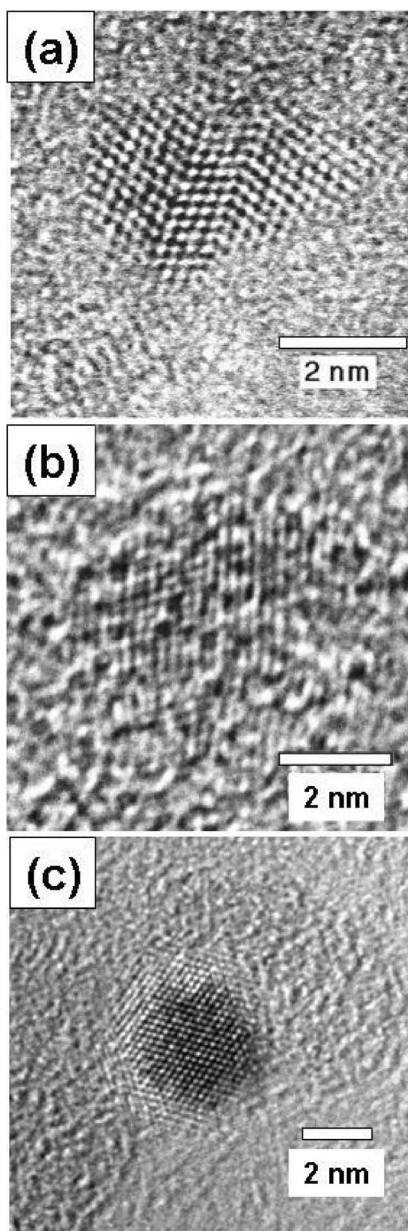
FIG. 1. TEM images obtained from three types of nanodiamond samples. (a) and (b): enlarged views of a selected Murchison (a) and Allende (b) meteorite diamonds, showing the characteristic lattice planes of 0.21 nm distance; (c) enlarged view of an individual synthetic diamond (UDD sample). (a) was provided by F. Banhart, (b) and (c) by P. van Aken.

$$r_{j+1} - r_j = k_j, \qquad (1)$$

the origin of lognormal growth must be sought in a proportionate (size-dependent) growth of the variate r_j,

$$r_{j+1} - r_j = k_j r_j. \qquad (2)$$

As a consequence, particle growth is accelerated for larger particle sizes, at the expense of smaller ones.

Equation (2) is considered to be an approximation because the growth factor k_j may contain inherent randomness.[21] This randomness can be implemented by the *law of*

proportionate effect (LPE),[2,21] where k_j is interpreted as a random number that varies between limits (e.g., between 0 and 1). Sorting this equation by k_j and subsequent summation results in the series of logarithmic size dependence,

$$\sum_{j=0}^{n} k_j = \sum_{j=0}^{n} \frac{r_{j+1} - r_j}{r_j} \approx \ln(r_n) - \ln(r_0), \qquad (3)$$

with initial and final particle radii r_0 and r_n, respectively. After re-sorting, the exponential form directly translates into the product form

$$r_n \approx r_0 \prod_j (1 + k_j) \qquad (4)$$

for small process step widths, $k_j \to 0$. Application of the multiplicative analogue of the Lindeberg-Levy theorem,[22,23] which states that the product of any sequence of independent, positive variate with the same probability distribution is asymptotically lognormally distributed, the lognormal size distribution f is obtained in its original form,

$$f(r) \equiv \frac{d\Lambda(r|\mu,\sigma^2)}{d\ln(r)} = \frac{1}{\sqrt{2\pi\sigma^2}} \exp\left(-\frac{1}{2\sigma^2}[\ln(r) - \mu]^2\right), \qquad (5)$$

where the prefactor accounts for a proper normalization of the distribution integral to unity. The scale parameter μ is identified with the expectation of $\ln(r)$, and σ represents a shape parameter of the distribution, as will be outlined in Sec. V. Here the function $\Lambda(r|\mu,\sigma^2)$ is commonly known as the "frequency curve" and represents the probability to find some specific value between r and $r+dr$. Hence, the variate r is denoted as a "Λ-variate."

lognormal size distributions have long been explained on the basis of Brownian coagulation models,[24,25] but it turned out later that essentially any process where the basic mechanism is particle diffusion and drifts through a finite region exhibits lognormal growth.[26] Here, the time available for particles to grow determines their peculiar size distribution.

III. SAMPLE PREPARATION AND CHARACTERIZATION

Synthetic ultradisperse diamonds (UDDs, type "CH7") were produced during detonations of a composite explosive (trotyl/cyclotrimethylene-trinitramine, TNT/RDX) in a hermetic tank filled with inert gas (nitrogen, argon) of varied partial nitrogen pressure.[9] The detonation parameters, e.g., the nitrogen pressure and the TNT/RDX ratio, were optimized to increase the UDD yield. Subsequently the UDDs were obtained as solid residue after soot oxidation with perchloric acid.

The cosmic diamonds were extracted from the meteorite samples by first dissolving the bulk material within a combined hydrochloric/hydrofluoric acid treatment This was followed by dissolving sulfur using carbon disulfide as well as destroying organic compounds with Na-dichromate. The residues were then washed with distilled water, and perchloric acid was used to oxidize surviving graphitic carbon. Finally, using ammonium hydroxide, the diamond fractions were extracted as colloids. In some cases, an additional treat-

ment with sulfuric acid was performed in order to dissolve additional oxidic minerals such as spinel ($MgAl_2O_4$). For identification the nanodiamond samples were suspended in Milli-Q water, and several drops of the suspension were dried on a TEM-copper grid coated with holey carbon film (Plano). The grid samples were then characterized by means of high-resolution transmission electron microscopy (HR-TEM, Philips TECNAI F30).

IV. MASS ANALYSIS OF NANODIAMOND SAMPLES

Mass distributions of the different nanodiamond samples were recorded by means of a MALDI-TOF spectrometer (Bruker REFLEX III) using matrix-free laser ablation/ionization in combination with time-of-flight mass analysis. For this, the diamond samples were suspended with distilled water and dried on a stainless steel target plate. Near ablation threshold measurements were performed for a conservative sample treatment during the laser induced (soft) ionization/vaporization process.

For ablation, a nitrogen laser (pulse duration ~4 ns, wavelength $\lambda \sim 337$ nm) was used in the moderate fluence range between 0.35 and 0.4 J/cm^2. Mass spectra were recorded in the linear flight tube of the reflectron-type TOF spectrometer. For each mass spectrum, 50 laser shots were applied to 12 different sample positions for the release of nanoparticles on a target spot of ~30 μm diameter. To reduce the amount of data recorded by means of the built-in 2 GHz digital transient recorder, 200 channels were binned to obtain one averaged data point.

V. RESULTS AND DISCUSSION

Nanodiamond samples of both cosmic and synthetic origin were analyzed. The mass spectra of nanodiamond fractions from the Murchison and from the Allende meteorites are shown in Figs. 2(a) and 2(b), respectively. The mass spectrum obtained from synthetic ultradisperse (UDD) diamonds is shown in Fig. 2(c). All mass spectra are characterized by a steep rise at lower masses and a rather weak descent to higher masses.

Prior to further statistical treatment, the lognormal distribution function will be discussed against the background of mass distribution measurements as well as in the context of former TEM size distribution measurements. It will be demonstrated that the particle masses, which are connected to the radius (with a lognormal distribution) by a power law, reproduce lognormality.

In the simplest case, nanodiamonds are approximated as spherical particles of an effective radius r.[16] Introducing a related density $\tilde{\rho} := 4\pi/3\rho$ from the mass density ρ, and a related quantity $\tilde{x} := \tilde{\rho}^{1/3} r$ such that the mass is given by $m = \tilde{x}^3$, the multiplicative reproduction property of the lognormal distribution[2] can be directly applied: Given the Λ-variate $\tilde{x}$ with the frequency curve $\tilde{\Lambda}(\tilde{x}|\mu_x, \sigma_x^2)$, the mass m also represents a Λ-variate with

$$\Lambda(m|\mu_m, \sigma_m^2) = \Lambda(m|3 \cdot \mu_x, 9 \cdot \sigma_x^2) = \tilde{\Lambda}(\tilde{x}|\mu_x, \sigma_x^2). \quad (6)$$

From this, the interesting property becomes apparent that the measurement of any physical quantity which is connected to
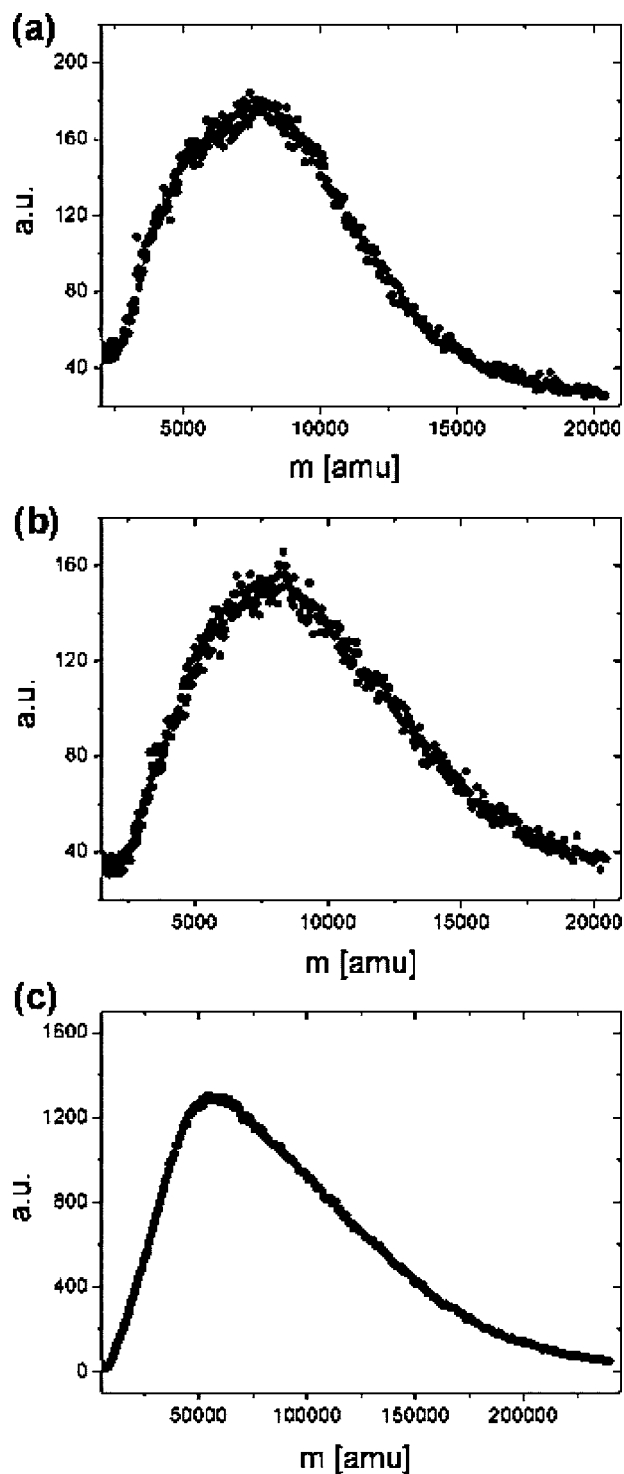
FIG. 2. Laser ablation/ionization time-of-flight mass spectra from the different nanodiamond samples: (a) Murchison, (b) Allende, and (c) synthetic diamonds. Each spectrum clearly exhibits a significantly asymmetric shape, as it is typical for lognormal size distributions.

a radius by a power law reproduces lognormality in the derived distribution, if the quantity radius itself is lognormally distributed. In this sense, size and mass distribution measurements are equivalent.

For further analysis, the statistical parameters of the mass distributions are extracted from probability plots (Fig. 3). After background subtraction, 10 data points each from the mass spectra were averaged to one point in the probability diagram. The horizontal axis represents the cumulative probability of the diamond masses, which are themselves given on the vertical logarithmic scale.

As outlined in Refs. 2 and 27, data which fit to a straight line within this probability representation are consistent with a lognormal distribution. The parametric straight line representation is given as

$$\ln(\xi) = \sigma_m \xi + \mu_m, \tag{7}$$

where the logarithm of the median mass, μ_m, is given by the $\ln(\xi)$ value at 50% of the cumulative probability,

$$\mu_m = \ln(\xi_{50\%}), \tag{8}$$

and the parameter σ_m is calculated from the ξ values at 16%, 50%, and 84% of the integral mass spectrum according to

$$\sigma_m = \ln\left(\frac{1}{2}\left[\frac{\xi_{50\%}}{\xi_{16\%}} + \frac{\xi_{84\%}}{\xi_{50\%}}\right]\right). \tag{9}$$

We obtain similar parameter values of $\sigma_m \sim 0.6$, ~ 0.55 and ~ 0.61 for the Murchison, Allende, and UDD samples, respectively.

In comparison with the synthetic diamonds, both cosmic samples consist of smaller particles, with a median mass

$$\langle m \rangle \equiv \exp(\mu_m)\,\mathrm{Da} \tag{10}$$

of $\langle m \rangle \sim 7$ kDa for the Murchison fraction and of $\langle m \rangle \sim 8.0$ kDa for the Allende fraction. The median mass of the UDD diamonds $\langle m \rangle \sim 65.2$ kDa is about an order of magnitude higher. In case of strong asymmetry, such as is typical for the lognormal distribution, the median distribution value has to be clearly distinguished from the mean value. For the lognormal distribution the mean value is given by

$$[m] \equiv \langle m \rangle \exp\left(\frac{1}{2}\sigma_m^2\right) = \exp\left(\mu_m + \frac{1}{2}\sigma_m^2\right), \tag{11}$$

which is significantly shifted to higher masses ($[m] \sim 8.4$ kDa for the Murchison diamonds, $[m] \sim 9.3$ kDa for the Allende diamonds, and $[m] \sim 78.5$ kDa for the UDD diamonds). It is also necessary to note that the parameter σ_m characterizes the shape of the distribution, and not its width. The distribution becomes almost symmetric for $\sigma_m \to 0$, and is highly asymmetric for $\sigma_m > 1$. The parameter σ_m differs from the standard deviation of the Λ-variate m which is given by ($w := \exp(\sigma_m^2)$)

$$\sigma_w \equiv \langle m \rangle \sqrt{w^2 - w}. \tag{12}$$

In contrast to the dimensionless shape parameter σ_m where the absolute mass scaling cancels, the quantity σ_w scales linearly with the median mass $\langle m \rangle$. We obtain $\sigma_w \sim 5.51$ kDa, ~ 5.46 kDa, and ~ 52.6 kDa for the Murchison, the Allende, and the UDD diamonds, respectively.

As is evident from the probability plots given in Figs. 3(a)–3(c), the main part of all data points follows the corre-
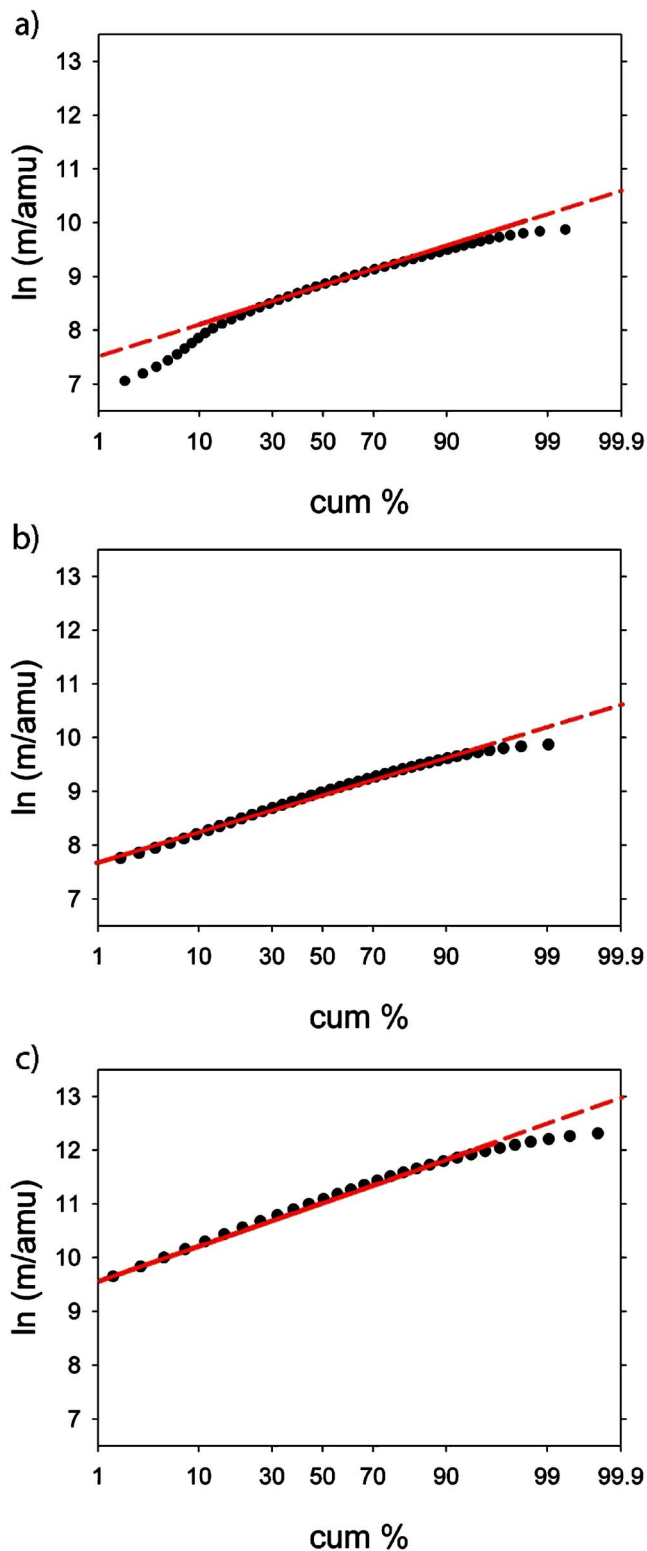
FIG. 3. (Color online) Probability plots extracted from the nanodiamond mass spectra from Fig. 2. Each point averages 10 data points from the mass spectrum. Straight lines are inserted for the emphasis of lognormal behavior within the major part of the cumulative axis. Deviations mainly towards higher masses are discussed in the text.

sponding straight lines rather well. Small deviations occur primarily for highest masses. Their overabundance might be ascribed to possible particle aggregation on the target or within the laser-induced vapor, and/or to possible impurities from higher (nondiamond) masses which survived the sample preparation procedure.

Since the median mass value rises with the expectation $E(1+k_j)$ of the growth factor k_j, and further, since the variance $D^2(1+k_j)$ augments the distribution width σ_w, some thermodynamic arguments can be formulated for a qualitative estimation of the distribution parameters. In our approach, the dimensionless process constant k_j is expected to be proportional to the collision rate, e.g., to the number of vapor phase collisions per process step, resp. per time increment. At any moment of the dynamical vapor phase evolution the carbon vapor is treated as an ideal gas. The validity of the approximation is supported by the fact that the process constant k_j needs to be small in order to obtain lognormal growth behavior [see Eq. (4)]. In the ideal gas regime the average thermal energy $\langle E \rangle \sim kT$ scales linearly with the square of the particle velocity $\langle v^2 \rangle_m$ averaged over all masses in the heterogeneous vapor. The average particle velocity further scales linearly with the inverse collision rate $\langle \tau^{-1} \rangle$, and hence linearly with the process constant k_j for the considered process step.

Under isochoric conditions, as they prevailed during UDD synthesis under laboratory conditions,[9] the relative influence of two different temperatures T_1 and T_2 is then found to change both the collision rate and the process constant k_j by a ratio of $(T_2/T_1)^{1/2}$. Simultaneously the pressure increases by a factor of T_2/T_1. In this way an increase in temperature leads to a higher collision rate, and finally to an increased particle growth rate. To resume, both the median particle mass $\langle m \rangle$ and the width of the mass distribution, σ_w, are expected to increase with increasing vapor temperature, resp. with increasing vapor pressure.

Within this simplified picture, the Murchison diamond fraction ($\mu_m \sim 8.85$, $\sigma_m \sim 0.6$, $\sigma_w \sim 5.51$ kDa) and the Allende fraction ($\mu_m \sim 8.99$, $\sigma_m \sim 0.55$, $\sigma_w \sim 5.46$ kDa) appear to have evolved in comparable temperature and/or pressure regimes. On the other hand, the synthetic nanodiamonds exhibit a much broader mass spectrum ($\sigma_w \sim 52.6$ kDa) which is shifted to significantly higher masses ($\mu_m \sim 11.09$, resp. $\langle m \rangle \sim 65.2$ kDa), but is similar in shape to the cosmic samples ($\sigma_m \sim 0.61$). This suggests conspicuously higher collision rates, and respectively higher temperatures and/or pressures, during their formation process. However, the mode of formation should be comparable in all cases as inferred from the nearly identical shape parameters.

The influence of parametric dependencies has been investigated experimentally during the synthesis of UDD nanoparticles. The synthetic diamonds have formed in a nitrogen atmosphere at pressures between 20–30 GPa and temperatures between 3000–4000 K during $\sim 10^{-6}$ s.[9] At such conditions the ideal gas approximation is reasonable for the inert nitrogen "carrier" gas atmosphere. Within their parametric study, Kuznetsov *et al.* have shown that an increase of partial nitrogen pressure effects higher mean UDD sizes, and further, that an increase of the temperature in the detonation zone leads to bigger UDD particles. Hence, both observations corroborate qualitatively our simple temperature and/or pressure model for diamond growth from vapor.

While the laboratory diamonds were produced under high pressure, the cosmic diamonds can be expected to have formed under much lower pressure as it is present in circumstellar space. Following our argumentation a strong reduction of the ambient pressure would indeed explain our observation that the median masses, i.e., distribution widths, of the cosmic diamonds take significantly lower values.

While the above considerations give some qualitative statement, further input is needed for an appropriate quantitative modeling of the diamond nucleation and growth processes in a vapor phase.

The parameter extraction from Fig. 3 further allows for a comparison to previous TEM particle size counting measurements. The size distributions of the meteoritic samples have been determined by Lewis *et al.*,[17] and also later by Daulton *et al.*[16] In both works, a median effective diameter of ~ 2.6 nm was determined for the Murchison diamonds,[16,17] and of ~ 2.8 nm for the Allende fraction.[16] However, a significantly lower median diameter of $\langle d \rangle \sim 1.0$ nm and a mean diameter of $[d] \sim 1.6$ nm, respectively, was obtained by Fraundorf *et al.*[28] for both Murchison and Allende diamonds (also in Ref. 11). These authors argue that an incomplete detection of smaller crystallites in Ref. 17 may have resulted in a distribution shift to higher masses.

Using a density of 3.52 g/cm^3 for crystalline diamond and assuming spherical diamond geometries, we calculate from our data a median effective diameter of ~ 1.9 nm for both Murchison and Allende diamonds. This value is located between the values from the different TEM investigations, but closer to that of Ref. 28.

In the case of the synthetic UDD sample CH7, a median effective diameter of 3.9 nm is calculated from the median mass of 65.2 kDa. This is in good agreement with the size determination by Kuznetsov *et al.*,[9] where an average UDD diameter between 3 nm and 5 nm has been determined, depending on the specific nitrogen pressure and the specific TNT/RDX ratio during synthesis.

In general, since TEM particle counting experiments are based on the two-dimensional particle projection onto the substrate surface, some systematic uncertainties are involved during the translation to the corresponding particle volume. Therefore, both the specific crystal structure and the orientation onto the substrate surface need to be considered.

Methodic uncertainties in the laser ablation method, on the other hand, arise, e.g., from possible fragmentation of intact diamonds during the laser irradiation process, as well as from possible laser-induced fusion of individual nanoparticles.

VI. CONCLUSION

We performed mass distribution measurements of different nanodiamond samples by means of laser ablation/ionization mass spectrometry. All samples exhibit lognormal mass distributions which are indicative for proportionate growth processes in the vapor phase, where the growth rate

crucially influences the particle size. Our results show good agreement to nanodiamond size distributions obtained from previous TEM investigations. Further the parameters of the mass distributions were qualitatively analyzed with respect to statistical considerations. More work will be required to establish profound quantitative models of the vapor phase nucleation processes.

*Corresponding author. Electronic mail: jmaul@uni-mainz.de

[1] L. B. Kiss, J. Söderlund, G. A. Niklasson, and C. G. Granqvist, Nanotechnology **10**, 25 (1999).

[2] J. Aitchison and J. A. C. Brown, *The Lognormal Distribution* (Cambridge University Press, Cambridge, England, 1969).

[3] Y. Kim, H. Sievering, J. Boatman, D. Wellman, and A. Pszenny, J. Geophys. Res. **100**, 23027 (1995).

[4] G. K. Yue, L. W. Thomason, L. R. Poole, P.-H. Wang, D. Baumgardner, and J. E. Dye, Geophys. Res. Lett. **22**, 2933 (1995).

[5] J. A. Koziol, J. Theor. Biol. **180**, 81 (1996).

[6] M. I. Marinov, Spectrosc. Lett. **17**, 1 (1984).

[7] R. S. Lewis, M. Tang, J. F. Wacker, E. Anders, and E. Steel, Nature **326**, 160 (1987).

[8] E. Zinner, Annu. Rev. Earth Planet Sci. **26**, 147 (1998).

[9] V. L. Kuznetsov, A. L. Chuvilin, E. M. Moroz, V. N. Kolomiichuk, Sh. K. Shaikhutdinov, Yu. V. Butenko, and I. Yu. Mal'kov, Carbon **32**, 873 (1994).

[10] W. C. Saslaw and J. E. Gaustad, Nature **221**, 160 (1969).

[11] E. Anders and E. Zinner, Meteoritics **28**, 490 (1993).

[12] D. D. Clayton, B. S. Meyer, C. I. Sanderson, S. S. Russell, and C. T. Pillinger, Astrophys. J. **447**, 894 (1995).

[13] A. G. G. M. Tielens, C. G. Seab, D. J. Hollenbach, and C. F. McKee, Astrophys. J. **319**, L109 (1987).

[14] J. A. Nuth III and J. E. Allen, Jr., Astrophys. Space Sci. **196**, 117 (1992).

[15] M. Ozima and K. Mochizuki, Meteoritics **28**, 416 (1993).

[16] T. L. Daulton, D. D. Eisenhour, T. J. Bernatowicz, R. S. Lewis, and P. R. Buseck, Geochim. Cosmochim. Acta **60**, 4853 (1996).

[17] R. S. Lewis, E. Anders, and B. T. Draine, Nature **339**, 117 (1989).

[18] E. Whitby and M. Hoshino, J. Electrochem. Soc. **143**, 3397 (1996).

[19] I. C. Lyon, V. A. Boote, and C. M. Davies, Meteorit. Planet. Sci. **36**, A119 (2001).

[20] D. McAlister, Proc. R. Soc. London **29**, 367 (1879).

[21] D. E. Kile and D. D. Eberl, Am. Mineral. **88**, 1514 (2003).

[22] P. Levy, *Calcul des Probabilités* (Gauthier-Villars, Paris, 1925).

[23] J. W. Lindeberg, Math. Z. **15**, 211 (1922).

[24] S. K. Friedlander and C. S. Wang, J. Colloid Interface Sci. **22**, 126 (1966).

[25] K. W. Lee, Y. J. Lee, and D. S. Han, J. Colloid Interface Sci. **188**, 486 (1997).

[26] J. Söderlund, L. B. Kiss, G. A. Niklasson, and C. G. Granqvist, Phys. Rev. Lett. **80**, 2386 (1998).

[27] N. A. J. Hastings and J. B. Peacock, *Statistical Distributions* (Butterworths, London, 1975).

[28] Ph. Fraundorf, G. Fraundorf, T. Bernatowicz, R. Lewis, and M. Tang, Ultramicroscopy **27**, 401 (1989).

[29] Recently we became aware of a related work based on Ref. 19: I. Lyon, Meteorit. Planet. Sci. **40**, 981 (2005).